




**Evidence for temperature chaos in spin glasses**Qiang Zhai <sup>1,\*</sup>, Raymond L. Orbach <sup>1,†</sup> and Deborah L. Schlage <sup>2</sup><sup>1</sup>*Texas Materials Institute, The University of Texas at Austin, Austin, Texas 78712, USA*<sup>2</sup>*Division of Materials Science and Engineering, Ames Laboratory, Ames, Iowa 50011, USA*

(Received 2 August 2021; revised 14 January 2022; accepted 19 January 2022; published 27 January 2022; corrected 1 March 2022)

We study the field cooled magnetization of a CuMn spin glass (SG) under temperature perturbations. The  $T$ -cycling curves are compared with the reference curve without temperature cycling. There is a crossover from the cumulative aging region to noncumulative aging region as the temperature change is increased. The cumulative aging range scales with the chaos length,  $\ell_c$ , becoming comparable to the correlation length,  $\xi$ , at the crossover boundary. The extracted chaos exponent,  $\zeta = 1.1$ , is in agreement with theoretical predictions. Our results strongly suggest temperature chaos exists in real SG systems.

DOI: [10.1103/PhysRevB.105.014434](https://doi.org/10.1103/PhysRevB.105.014434)**I. INTRODUCTION**

The equilibrium spin configuration in the spin glass (SG) phase [1–3] is predicted to reorient for arbitrarily small temperature variations on a length scale greater than  $\ell_c(T_1, T_2)$ , the chaos length [3,4]. The temperature chaos (TC) effect was first exhibited through a renormalization group approach [5,6] and  $T = 0$  fixed-point scaling arguments [3,4]. It has been studied analytically [7–16] and observed through simulations [17–20] on different lattice structures [21–29] by utilizing improved computable lattice sizes [30] and strategies [31–37] in both droplet-like [38–41] and replica symmetry-breaking scenarios [42,43]. Apart from the many results obtained at equilibrium, a recent simulation study [44] exhibited the evidence of TC in nonequilibrium states using the Edwards-Anderson Ising SG model.

In contrast with the relevant accomplishments in theoretical studies, the experimental verification [45–50] of TC remains controversial [51–54]. Because of sluggish glassy dynamics, experiments on SGs work exclusively in a nonequilibrium regime, accompanied by aging (logarithmically slow relaxation) [55–58], rejuvenation [59,60], and memory effects (recovery of the response generated at a temperature stop before successively cooling and heating back to the original temperature) [61–63]. It has been argued that rejuvenation, a renewal of the aging process (or a discontinuity in exploring phase space), can occur without invoking TC. Doubts [64–66] have been cast on these latter claims [67–70], because such findings could be obtained by tuning of parameters [71] or be camouflaged by small timescales, lattice size [72], and cooling rates effects [73] in simulations. It has been argued further that a second rejuvenation [71,74], under the protocol when the system is cooled to a lower temperature and then heated back, should be understood within the formalism of TC. A well-established picture of TC in SGs will contribute to a better understanding of similar phenomenon in more

general random systems [75–80] and to developing quantum annealers [81–84].

Here we take rejuvenation [49,85] in the aging process of the field cooled (FC) magnetization as a sign of the onset of TC. The experimental protocol we employ involves a temperature cycling process, whence the rejuvenation effect should be classified as second rejuvenation. We calibrate the chaos length using the correlation length,  $\xi$ , a measure of the size of glassy domains [86], controlled by the varied initial temperature  $T_1$  and fixed aging time  $t_1$ . The scaling relation between the chaos length and the *reversible temperature range*  $\delta T^{\text{rev}}$ , where the aging is cumulative between two temperatures in a  $T$ -cycling process, is shown to be satisfied. A chaos exponent  $\zeta$  [4] close to the theoretical value of unity is extracted. These results strongly suggest the existence of TC in the canonical CuMn SG.

The remainder of the paper is organized as follows. We present the experimental protocol in Sec. II. The transition from cumulative aging to noncumulative aging is exhibited in Sec. III. The chaos exponent  $\zeta$  is extracted and compared with theoretical values in Sec. IV. We give a discussion and the conclusion in Sec. V. The technical details are given in the Appendixes.

**II. EXPERIMENTAL PROTOCOL**

The underlying premise behind our experiments is based on a length scale argument. In the absence of TC, aging at two temperatures  $T_1$  and  $T_2$  contributes cumulatively to the growth of the correlation length at each temperature. In the presence of TC, the correlation growth at  $T_1$  cannot be projected onto the growth of the correlation length at  $T_2$  and vice versa. For example, consider aging at  $T_1$  to generate a certain correlation length,  $\xi(T_1)$ . On changing the temperature to  $T_2$ , instantaneously  $\xi(T_2) = \xi(T_1)$ . If  $\ell_c(T_1, T_2)/\xi(T_1) \geq 1$ , aging at  $T_2$  continues the correlation length growth from  $\xi(T_1)$ . If, however,  $\ell_c(T_1, T_2)/\xi(T_1) < 1$ , the system experiences incoherent spin-flipping dynamics. In  $T$ -cycling experiments, the situation is further complicated because, during the process of heating the system back to  $T_1$ ,  $\xi(t)$  is changing

\*qiang@utexas.edu

†orbach@utexas.edu

TABLE I. The extracted reversible cumulative aging range  $\delta T^{\text{rev}}$  and the effective aging time  $t_2^{(T_1)}$  for different  $T_1$ . The data are sampled every 100 s; the time translation used to overlap to the reference curve is multiples of 100 s.

$T_1$ (K)	18	17	16	15	14
$\delta T^{\text{rev}}$ (mK)	450	510	600	690	800
$t_2^{(T_1)}$ (s)	2000	2000	2500	3000	1500

with time, while the chaos length  $\ell_c(T_1, T_2)$  is fixed by the temperature separation. This complication will be discussed in detail below.

We chose working with the FC magnetization [87], the magnetization response of a sample aged in a constant field without field change after being cooled to  $T_1$  from above  $T_g$ , rather than conventional alternatives like zero-FC (ZFC) [88,89] magnetization or thermoremanent magnetization [85,90]. This is to eliminate the possible chaos induced by a magnetic-field change [91,92].

Our specific protocol consists of two parts: One to measure the FC magnetization,  $M_{\text{FC}}(t, T_1, H)$ , without a temperature perturbation as the *reference curve* and the other with temperature cycling to study cumulative aging and TC. The reference curve was measured by cooling the sample from 40 K, well above  $T_g$ , the SG condensation temperature, to the measurement temperature,  $T_1$ , in a constant field  $H = 40$  Oe at 10 K/min. After the temperature was stabilized at  $T_1$  for 100 s, the reference curve magnetization,  $M_{\text{FC}}^{\text{ref}}(t, T_1)$ , was recorded.

In the  $T$ -cycling experiment, the sample was cooled from 40 K to  $T_1$  at 10 K/min, and the magnetization was recorded under the same temperature stabilization condition for a duration of  $10^4$  s. For clarity, the first aging period is denoted as  $t_1$ , and the instantaneous point in time before dropping the temperature further is referred to as  $\hat{t}_1$ . After  $\hat{t}_1$ , the temperature was lowered to  $T_2 = T_1 - \Delta T$ . The temperature cooling rate was adjusted to lie between a range from 8 to 100 mK/min in order to minimize temperature downshoot after reaching  $T_2$ . After  $t_2^{(1)} = 10^3$  s aging at  $T_2$ , the sample was heated back with a symmetrical heating profile to  $T_1$ , again avoiding temperature overshoot.

It should be noted that because of the finite cooling rates, the correlation length will continue to grow during the cooling and heating process. The time spent in the cooling and heating process between  $T_1$  and  $T_2$  is denoted as  $t_2^{(2)}$  of the order of 100 s. Together with  $t_2^{(1)}$ , the total time spent during temperature cycling would be  $t_2 = t_2^{(1)} + t_2^{(2)}$ . The magnetization was recorded 100 s after the temperature was stabilized at  $T_1$  during the period  $t_3$  and was denoted as  $M_{\text{FC}}^{\text{cyl}}(T_1, t_3; T_2, t_2; T_1, t_1)$ . It should be emphasized that the magnetization measurements were conducted during  $t_1$  and  $t_3$  at  $T_1$  only. More details of the experimental protocol are provided in Appendix A.

One needs an appropriate method to characterize the reference curve and the  $T$ -cycling curve in order to interpret the experimental results. Traditionally, a collapse of a family of curves to a master curve [85] and the effective aging time [49],  $t_w^{\text{eff}}$  [defined as the time when the relaxation curve,  $S(t) = dM(t)/d\log(t)$ , peaks], have been used to characterize the aging curves. The former needs additional parametriza-

tion in order to convert the physical time into reduced time [93]. For the latter, the time at which  $S(t)$  peaks becomes more difficult to extract for long waiting times, as the  $S(t)$  curve broadens substantially. Moreover, the relaxation curve is measured under a change of magnetic field. The effective aging time is reduced as a function of field and correlation length [94,95], leaving the assumption that  $t_w \sim t_w^{\text{eff}}$  [49] to be somewhat precarious for large values of  $\xi$ , where  $t_w$  is the time before a field is switched on or off. This may explain why the data points do not overlap well at the timescale of  $10^5$  s in the cumulative aging range reported in Ref. [49]. Along with possible magnetic-field-induced chaos, these factors may be responsible for their small value of  $\zeta$  that lies well outside the theoretical estimates.

Because TC has been reported to be a subtle [43] and gradual [34] effect, we have chosen to overlap the cycling curve and reference curves directly. The drawback of our approach is the vulnerability of signal quality to external noise. A squid signal jump caused by environment noise ruins a set of measurements. Note that before  $\hat{t}_1$ , there is no difference in protocols between the reference curve and the  $T$ -cycling curve measurements;  $M_{\text{FC}}^{\text{cyl}}(T_1, t_1)$  and  $M_{\text{FC}}^{\text{ref}}(t)$  can be overlapped directly. After  $\hat{t}_1$ , if a time translation  $\delta t$  can be found, such that  $M_{\text{FC}}^{\text{cyl}}(T_1, t_3 + \delta t; T_2, t_2; T_1, t_1) = M_{\text{FC}}^{\text{ref}}(t, T_1)$ , the aging can be taken as cumulative and reversible. Otherwise, when the overlap process fails, rejuvenation is signaled as a consequence of TC.

The sample used in our experiments is a 6 at. % CuMn single crystal [96] grown at the Ames Lab with a SG transition temperature  $T_g = 31.5$  K. Details of the preparation of the sample can be found in Appendix C. The magnetization measurements were taken on a Quantum Design commercial superconducting quantum interference device. The temperature sensor is located within 5 mm of the sample.

### III. THE TRANSITION TO TC

In order to observe the transition from cumulative aging to noncumulative aging (i.e., TC), we fixed  $T_1$  and gradually lowered the temperature  $T_2 = T_1 - \Delta T$  in a series of measurements until the  $T$ -cycling curves could no longer be overlapped with the reference curve. Initially, the  $\Delta T$  was reduced at 100 mK steps to locate a rough onset of TC. Because the temperature resolution of our measurement was  $\pm 5$  mK, a 10 mK temperature step was used thereafter to determine a more accurate boundary between reversible cumulative aging and noncumulative aging. A typical example is shown in Fig. 1 at 18 K, where the approximate magnitude of reversible range is  $\delta T^{\text{rev}} = 450$  mK. The same process was repeated for different values of  $T_1$  down to 14 K. The reversible cumulative aging temperature ranges are listed in Table I. A complete set of data for all the measured temperatures can be found in Appendix D.

The underlying physical process can be described by a competition between the correlation length  $\xi$  and the chaos length  $\ell_c(T_1, T_2 = T_1 - \Delta T)$ . After aging at  $T_1$  for a period of  $t_1$ , the correlation length reaches  $\xi(T_1, t_1)$ , as described by either power-law growth [86,97] or logarithmic growth [98] for the droplet-scaling model [2]. For brevity, we consider

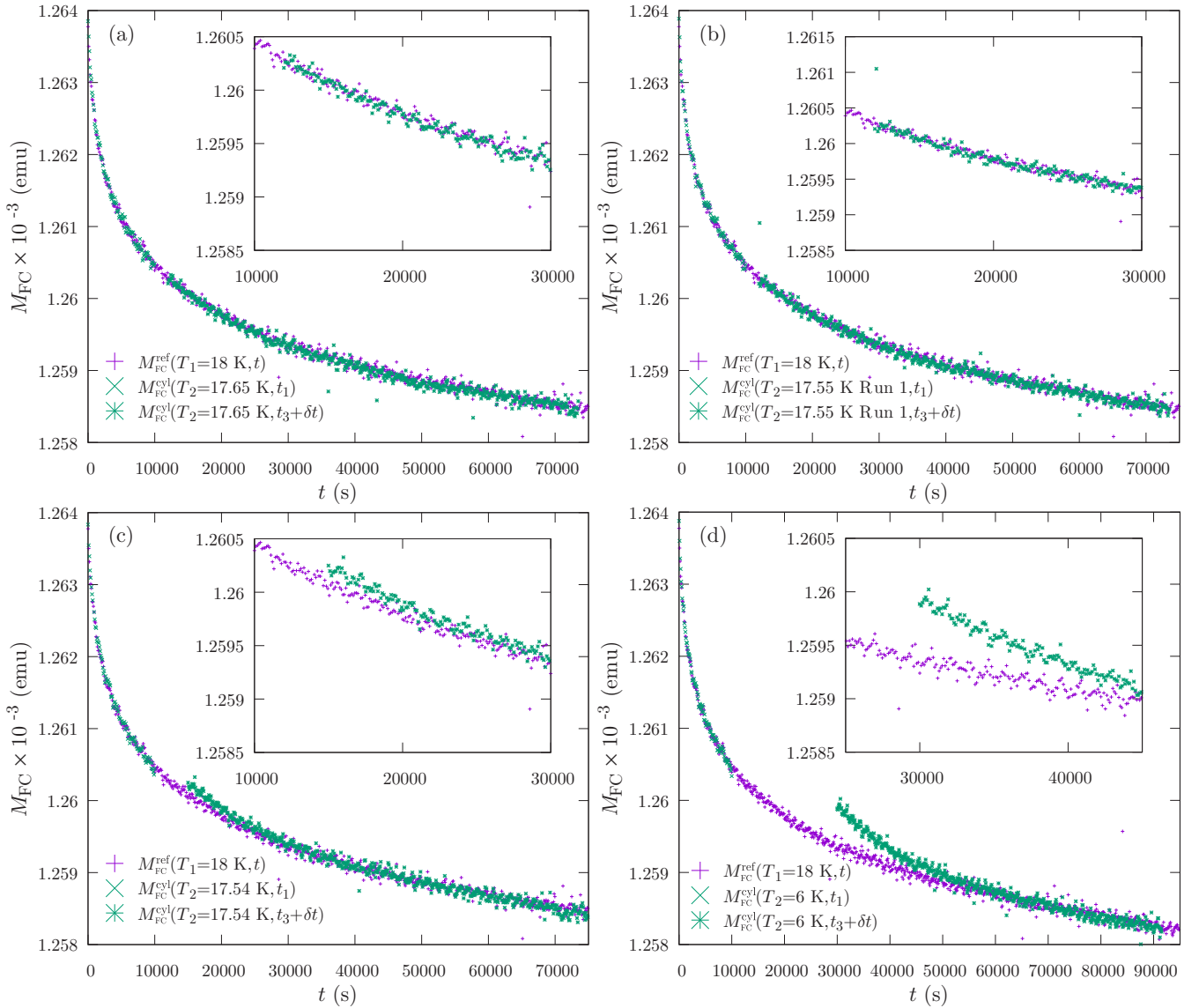


FIG. 1. The example of  $T_1 = 18$  K. The temperature is gradually lowered to  $T_2$  after  $t_1 \approx 10^4$  s and heated back after  $t_2^{(1)} \approx 10^3$  s. The  $T$ -cycling curve is then shifted by  $\delta t$  to overlap the reference curve. In the reversible temperature range, (a) and (b), the cycling curve can be overlapped with the reference curve over the whole period  $t_3 \approx 7 \times 10^4$  s. In the chaotic range, (c) and (d), the cycling curve can only be partially overlapped. Thus we conclude that, at  $T = 18$  K, TC sets in for  $\Delta T > 450$  mK.

power-law dynamics with a similar analysis for the other. Following a temperature drop, if

$$x_1 = \ell_c(T_1, T_2)/\xi(T_1, t_1) \geq 1, \quad (1)$$

the correlation length will continue to grow. The time taken in the cooling process has been omitted in the above expression.

However, one should be aware that the aging rates of  $\xi$  at  $T_1$  and  $T_2$  are, in general, different. According to the power-law growth rate,  $\xi(t, T) = b(t/\tau_0)^{1/z(T)}$ , where  $b$  is a geometrical factor,  $1/\tau_0 \sim k_B T_g/\hbar$  is the exchange attempt frequency, and the exponent  $z(T)$  sets the aging rate. The factor,  $z(T)$  [99], is linearly dependent on  $T$  and has the form  $z(T) = z_c T_g/T$ , where  $z_c$  [96] can be approximately taken as a constant over our temperature range. For cumulative aging, the aging time  $t_1$  at  $T_1$  can be effectively converted to aging time  $t_1^*$  at  $T_2$

through

$$(t_1/\tau_0)^{T_1} = (t_1^*/\tau_0)^{T_2}. \quad (2)$$

After the aging period  $t_2$  at  $T_2$ , the correlation length reaches approximately

$$\xi(T_2, t_2; T_1, t_1) \approx b[(t_1^* + t_2^*)/\tau_0]^{T_2/(z_c T_g)}, \quad (3)$$

in which  $t_2^{(2)}$  can be projected to an effective aging time  $t_2^{(2*)}$  at  $T_2$ , and  $t_2^* = t_2^{(1)} + t_2^{(2*)}$  if Eq. (1) holds.

Whether aging is cumulative or not, upon heating the system back to  $T_1$  depends on the variable

$$x_2 = \ell_c(T_1, T_2)/\xi(T_2, t_2; T_1, t_1). \quad (4)$$

Again, if  $x_2 \geq 1$ , the correlation length growth continues, and cumulative aging results in an overlap of the reference curve and the cycling curve over the full experimental time

period. Either the opposite of Eq. (1) or  $x_2 < 1$  in Eq. (4) will result in a chaotic reorientation of the spin configuration. Thus, in general, the measured reversible range  $\delta T^{\text{rev}}$  is a function of  $(T_1, t_1)$  that sets the correlation length before the temperature drop to  $T_2$ , and  $(T_2, t_2)$  that sets the correlation length growth during the temperature cycling period.

#### IV. EXTRACTION OF THE CHAOS EXPONENT $\zeta$

TC was initially introduced through a renormalization group argument. In that context, we shall use the associated scaling arguments for the extraction of  $\zeta$ . The chaos length (overlap length)  $\ell_c(T_1, T_2)$  is the length scale within which the spin correlations are free of the influence of temperature variation. For small temperature changes, the free energy at temperature  $T_1$  [3] is approximated from the free energy at  $T_2$  through a Taylor expansion,

$$F(T_1) \approx F(T_2) - (T_1 - T_2)S(T_2), \quad (5)$$

where  $F(T) = \gamma(T)\ell^\theta$ , and  $S(T) = \sigma(T)\ell^{d_s/2}$ , the droplet interface free energy and entropy, respectively. Here,  $d_s$  is the surface fractal dimension [3]. Alternatively, noticing that the energy term is similar at the two temperatures at the chaos length scale [32],

$$F(T_1) \approx F(T_2) + T_2 S(T_2) - T_1 S(T_1). \quad (6)$$

On a sign change of the free energy at  $T_1$ , the above approximations in Eqs. (5) and (6) yield

$$\ell_c(T_1, T_2) = \left[ \frac{\gamma(T_2)}{(T_1 - T_2)\sigma(T_2)} \right]^{1/(d_s/2 - \theta)},$$

$$\ell_c(T_1, T_2) = \left[ \frac{\gamma(T_2)}{T_1\sigma(T_1) - T_2\sigma(T_2)} \right]^{1/(d_s/2 - \theta)}. \quad (7)$$

Thus the chaos exponent,  $\zeta = d_s/2 - \theta$ , and  $S(T)$  is proportional to  $\sqrt{T}$  [72].

To extract a value for  $\zeta$ , we assume that the length scale  $\ell_c(T_1, T_2) \approx \xi_c$  at the boundary between cumulative aging and noncumulative aging. Here  $\xi_c$  is the correlation length when the system is heated back to  $T_1$ , and  $T_1 - T_2 = \delta T^{\text{rev}}(T_1, T_2)$ . For power-law growth,  $\xi_c = ba_0(t_c/\tau_0)^{T/(z_c T_g)}$ , where  $t_c$  is the timescale used to estimate  $\xi_c$ . Recall that, in the reversible range, the cycling curve can be overlapped with the reference curve after a time translation. The time difference between the first point of the translated curve measured during  $t_3$  and  $\hat{t}_1$  is denoted by  $t_2^{(T_1)}$ , the time taken as the effective aging time over the period of  $t_2$ . The sum of  $t_2^{(T_1)}$  and  $t_1$  is used for  $t_c$  at the crossover boundary (the lowest temperature drop without rejuvenation). The exponent  $z_c = 12.37$  [96] was measured on the same sample. The scaling relation between  $\ell_c(\xi_c)$  and the temperature drop, following Eq. (7), is exhibited in Fig. 2, with  $\zeta \approx 1.1$  for two different approximation schemes. This value is within the range of well-accepted values for  $\zeta$  that scatter around unity from theoretical calculations and simulations [32,34,36,44,100] for the 3D Ising model. Specific values of the chaos exponent from literatures are provided in Appendix B.

For logarithmic growth, the correlation length would grow as  $\xi_c = ba_0[\log(t_c/\tau_0)k_B T/\Delta(T)]^{1/\psi}$ , where  $\Delta(T)$  is the free-

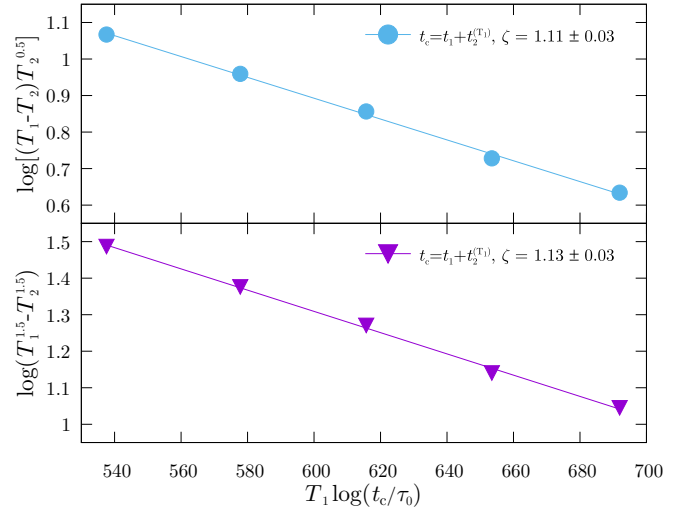


FIG. 2. Using a power-law growth for  $\xi$ , the chaos exponent  $\zeta \approx 1.1$  is extracted for different approximation schemes following Eq. (7).

energy barrier for the thermal-activated process [49]. Using the same choice of  $t_c$  and assuming  $\Delta(T)$  does not vary too much, the fitted curve in Fig. 3 gives the ratio  $\zeta/\psi \approx 1.7$ . By requiring  $\zeta = 1.1$ ,  $\psi \approx 0.65$ , in the range of reported values [94,101] for the droplet model.

#### V. DISCUSSION AND CONCLUSION

The concept of TC was introduced in the context of equilibrium properties [3,4]. Nevertheless, the glassy domain characterized by the correlation length formed toward equilibrium should be indistinguishable from that in equilibrium. Moreover, the concept of TC has been shown to exist under a nonequilibrium condition [44]. Further, the idea of TC is compatible with other prominent theories of SGs [34,42,44]. Beyond that, the analogy of TC is widely reported in more general frustrated complex systems, for example, with  $\zeta = 1$

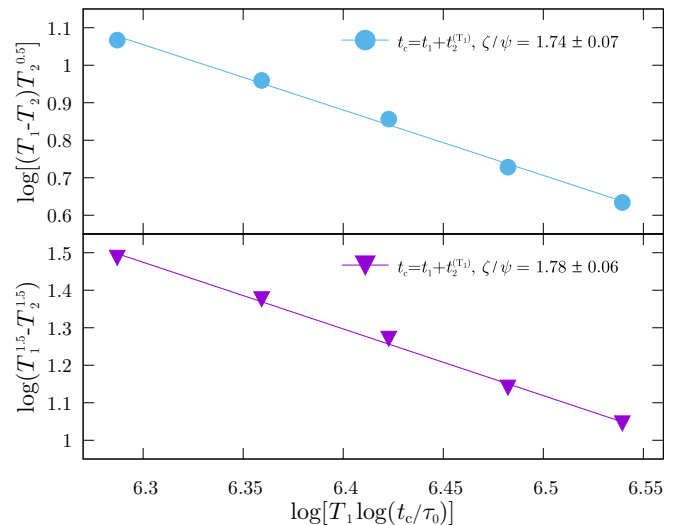


FIG. 3. Using a logarithmic growth law of  $\xi$ , the ratio of  $\zeta/\psi \approx 1.7$  compared with the power-law growth result is shown in Fig. 2.

for the disordered Bose fluid [80]. Although the value of  $\zeta$  appears to vary for different physical systems (see a different reported value for elastic media [75]), the scaling law between  $\ell_c$  the chaos length and an external perturbation may well be general.

Though CuMn is often categorized as a metallic Heisenberg system, the introduction of anisotropy (because, e.g., of the omnipresent Dzyaloshinskii-Moriya interaction) [102,103] breaks the rotational symmetry and makes the system one of Ising universality. In addition, Ising behavior of CuMn has been affirmed through the synergy between experiments and simulations [104,105].

With only one free variable,  $z_c$ , in the power-law approximation (actually a measured value for the identical sample), the closeness between the extracted chaos exponent and theoretical values from the Ising model calculations and simulations is striking. The crossover from cumulative aging to noncumulative aging is therefore well explained within the framework of TC. Although other possible explanations to the rejuvenation phenomena cannot be ruled out, we believe our findings provide strong evidence for TC in a real SG system.

### ACKNOWLEDGMENTS

We thank the very helpful communications with Prof. Victor Martin-Mayor. This work was supported by the U.S. Department of Energy, Office of Science, Office of Basic Energy Sciences, Division of Materials Science and Engineering, under Award No. DE-SC0013599. Part of the research was performed at the Ames Laboratory, which is operated for the U.S. DOE by Iowa State University under Contract No. DE-AC02-07CH11358.

### APPENDIX A: THE PROTOCOL AND MEASUREMENTS

To clarify the notation for the FC temperature-cycling measurements reported in the paper, a schematic plot of the experimental protocol is shown in Fig. 4. The measurements were conducted on a Quantum Design MPMS machine with a superconducting magnet. Before each set of measurements, the magnet field was oscillated from 1 T to 0 Oe to reduce any remanent field. A paramagnetic sample was measured at 300 K to establish the compensating field required for a zero

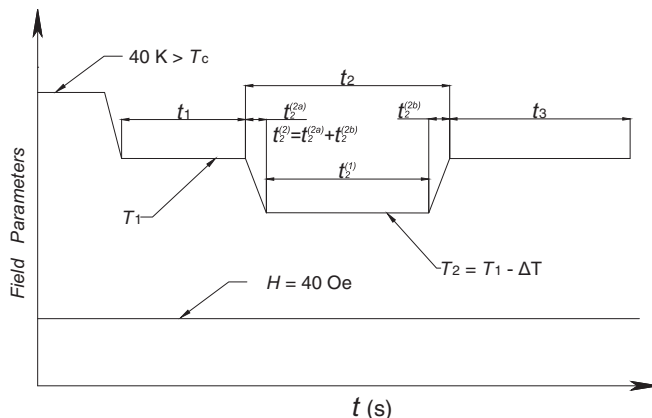


FIG. 4. Schematic plot of the FC magnetization  $T$ -cycling experimental protocol. The time duration ratio is exaggerated for clarity.

TABLE II. The chaos length  $\ell_c(T_1, T_2)$  is proportional to  $|T_1 - T_2|^{-1/\zeta}$ , defining the chaos exponent  $\zeta$ . It has been studied extensively theoretically, but there are few direct experimental measurements. The values of  $\zeta$  listed in the table range from 0.7 to 1.2. The only experimental study [49] known to the authors reported  $\zeta = 0.385$ .

Reference	$\zeta$	Notes
[8]	1	Mean-field Ising SG, analytical
[18]	$1.0 \pm 0.2$	2D Ising, simulation
[22]	0.85	2D Ising, numerical
[49]	0.385	AgMn, experimental
[72]	1.01, 1.15	3D Ising SG, numerical
[39]	0.745	Migdal-Kadanoff approach, simulation
[41]	$1.12 \pm 0.05$	4D EA Ising SG, simulation
[26]	$0.95 \pm 0.05$	2D Ising SG, numerical
[32]	1.04	3D Ising SG, numerical
[20]	0.7–1	Various lattice model, simulation
[34]	1.06	3D Ising SG, simulation
[36]	0.96(5)	3D Ising SG, simulation
[106]	1.19(7)	4D Ising SG, simulation
[44]	1.19(2)	3D Ising SG, simulation

magnetization response. The CuMn sample was preserved in liquid nitrogen before usage.

### APPENDIX B: REPORTED TC EXPONENT $\zeta$ IN VARIOUS SG MODELS

Values for the chaos exponent  $\zeta$  from numerical studies, simulations, and experiment are listed below in Table II.

### APPENDIX C: THE SAMPLE DETAILS

The details for the sample preparation are already reported in Ref. [96]. For the reader's convenience, we reproduce the description here.

Crystal growth and sample preparation were carried out by the Materials Preparation Center (MPC) of the Ames Laboratory, USDOE. Cu from Luvata Special Products (99.99 wt. % with respect to specified elements) and distilled Mn from the MPC (99.93 wt. % with respect to all elements) were arc-melted several times under an Ar at atmosphere and then drop-cast into a water-chilled copper mold. The resulting ingot was placed in a Bridgman-style alumina crucible and heated under vacuum in a resistance Bridgman furnace to 1050 °C, just above the melting point. The chamber was then backfilled to a pressure of 60 psi with high-purity argon to minimize the vaporization of the Mn during growth. The ingot was then further heated to 1300 °C and held for 1 h to ensure complete melting, and for the heat zone to reach a stable state. The ingot was withdrawn from the heat zone at a rate of 3 mm/h. About 1/3 of the crucible stuck to the alloy. The ingot was finally freed after alternating between hitting with a small punch and a hammer and submerging in liquid nitrogen.

Cross-sections 1–2 mm thick were taken from near the start of the crystal growth and from the end for characterization. One side of each was polished and examined optically and with x-ray fluorescence (XRF). From the XRF measurements,

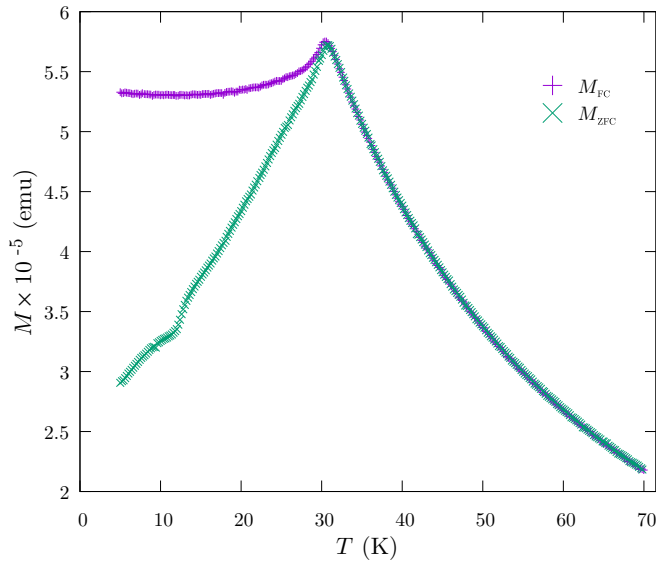


FIG. 5. The SG transition temperature  $T_g$  is determined by measuring the ZFC and FC magnetization in a small magnetic field. The ZFC and FC magnetization differs from one another at  $T_g$ , approximately 31.5 K for our sample.

the sample was found to be a single phase and at the end of the growth to be Mn rich. The samples were then etched in a 25% by-volume solution of nitric acid in water. Optically, the start of the growth was a single phase, single crystal, while the

end of the growth had large grains with a second phase along the grain boundaries. Small pits were seen both optically and by XRF. The pits could be minimized by varying polishing techniques but not gotten rid of.

Only the body portion of the crystal growth was used for the experiments. The ends of the growth were looked at as part of the characterization. They were not used because the end of the growth contained multiple grains and a second phase. An additional examination of the body was done to ensure that enough of the body had been cut away so as to remove the unwanted parts. The small shallow grains that remained on one end of the body were avoided when cutting the sample to be measured. As mentioned above, the XRF showed the body of the crystal growth to be a single phase. The composition gradient was gradual and smooth, and there was no evidence of Mn inhomogeneity seen in either the XRF or the optical characterization. The quality of the single crystal can be ascertained from Fig. 5. The peak in the ZFC magnetization is quite sharp and falls at the knee of the FC magnetization.

#### APPENDIX D: TRANSITION TO CHAOS DATA SETS

In this section, the data sets used to determine the boundary between reversible cumulative aging and noncumulative chaotic aging are given for each of the initial temperatures ( $T_1 = 18$  K in Fig. 6, 17 K in Fig. 7, 16 K in Fig. 8, 15 K in Fig. 9, and 14 K in Fig. 10).

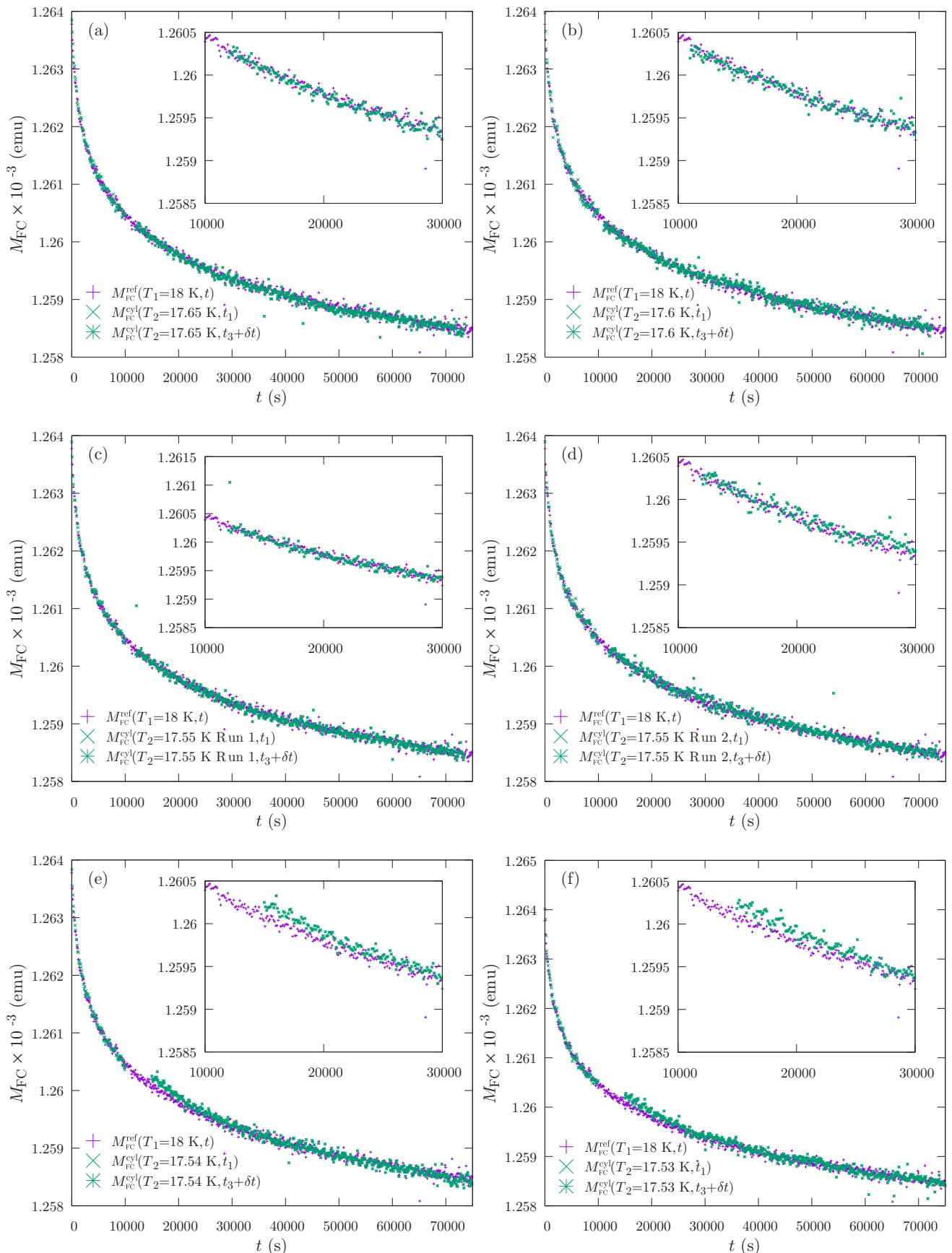


FIG. 6.  $T$ -cycling experiment results at  $T_1 = 18 \text{ K}$ . Cumulative aging is seen for plots (a) to (d). Noncumulative aging (chaos) begins in plot (e) and becomes larger for lower  $T_2$  in plots (f)–(k). The reversible temperature range is approximately 450 mK.

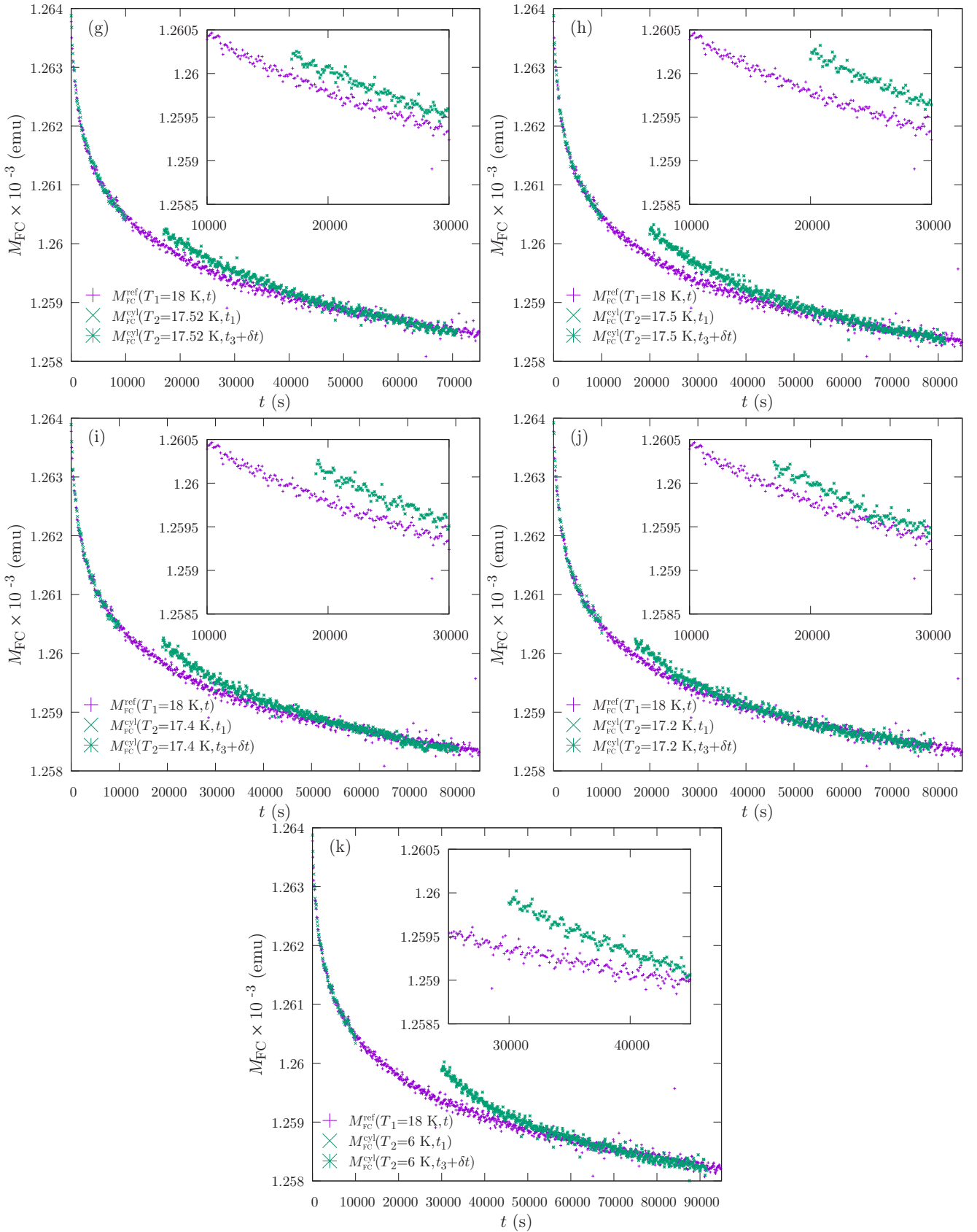


FIG. 6. (Continued.)



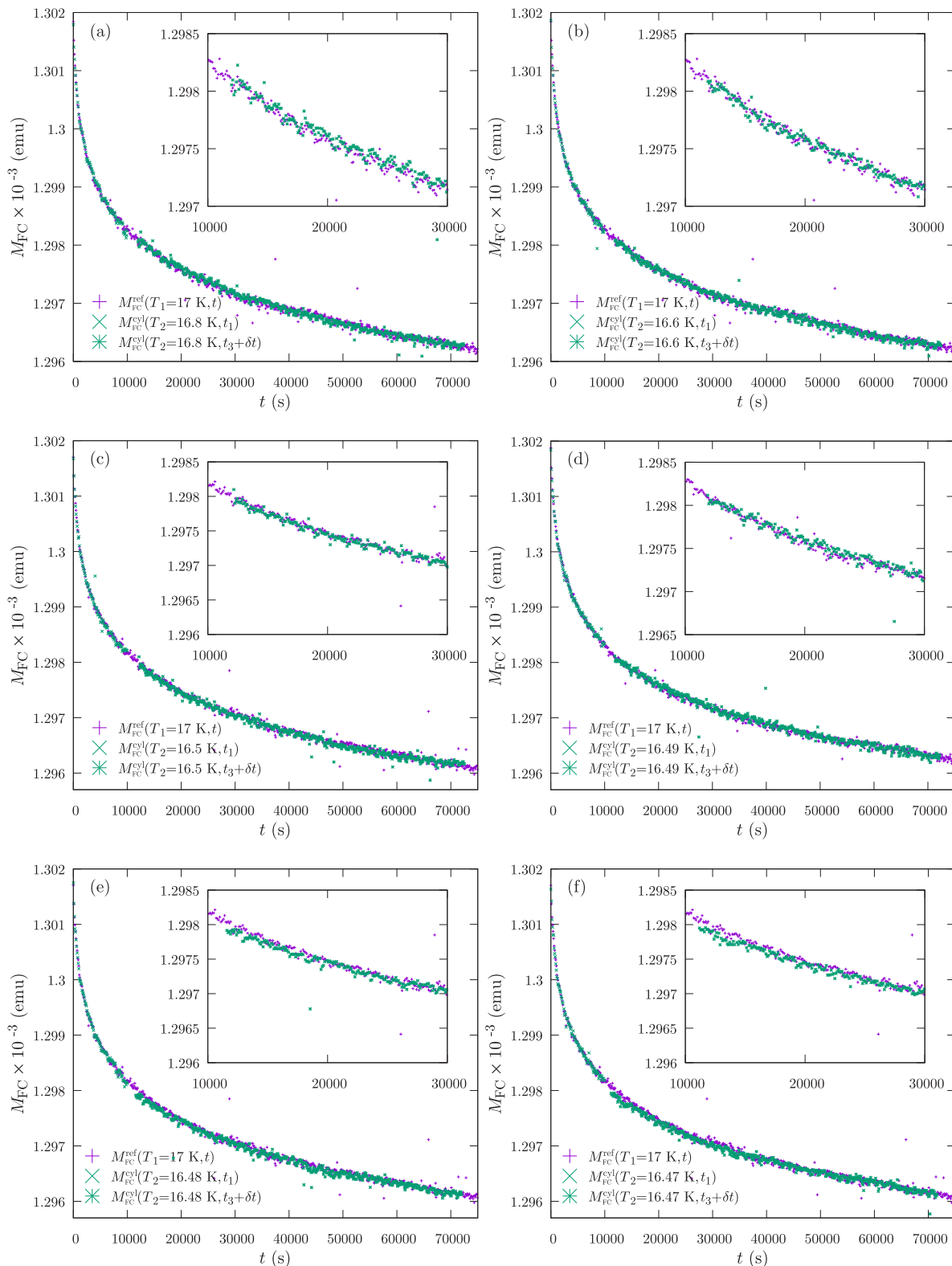


FIG. 7.  $T$ -cycling experiment results at  $T_1 = 17$  K. Cumulative aging is observed for plots (a)–(d); noncumulative aging is seen for (e) and (f). The reversible temperature range is approximately 510 mK.

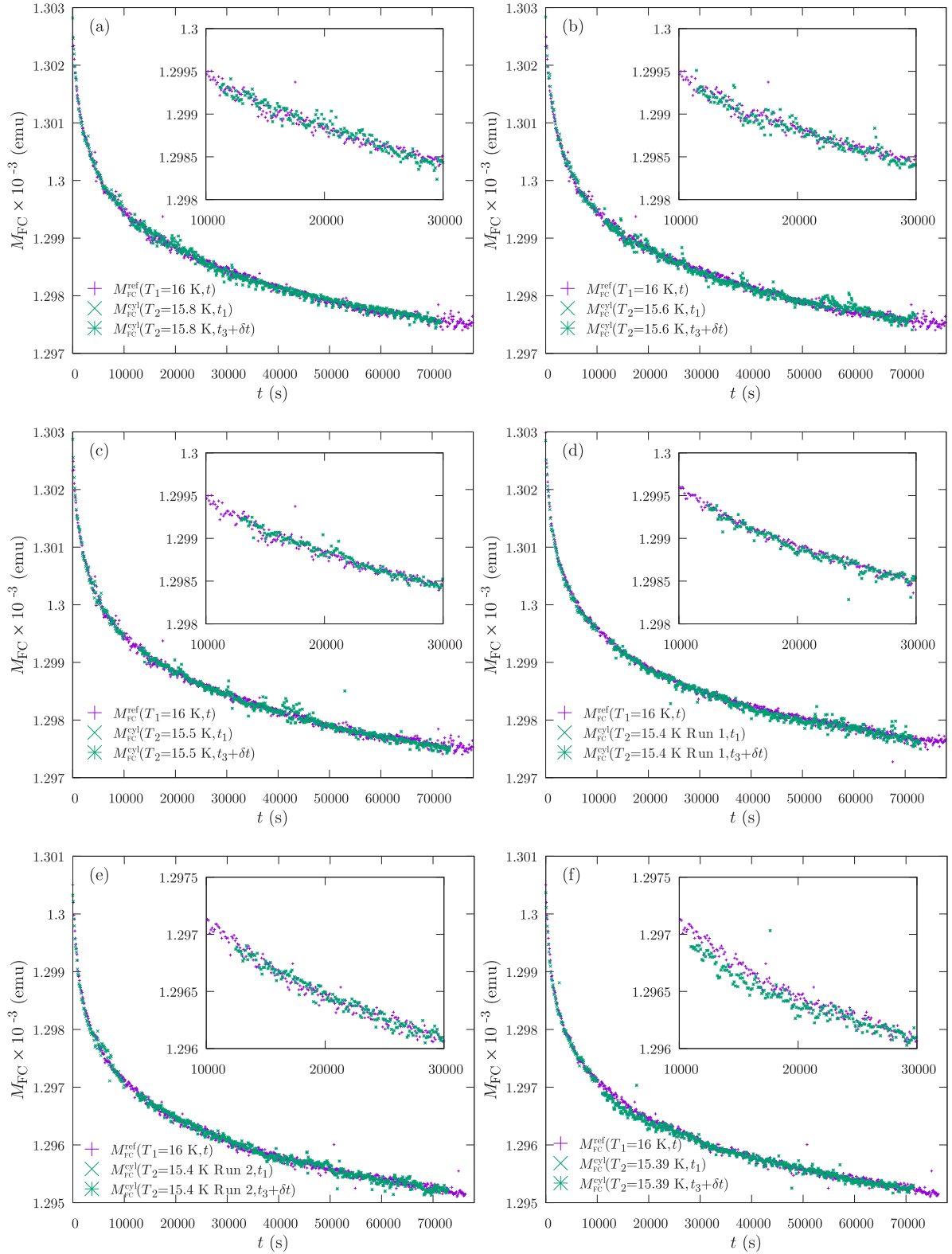


FIG. 8.  $T$ -cycling experiment results at  $T_1 = 16$  K. Cumulative aging is shown in plots (a)–(e); noncumulative aging begins in (f). The reversible temperature range is approximately 600 mK.

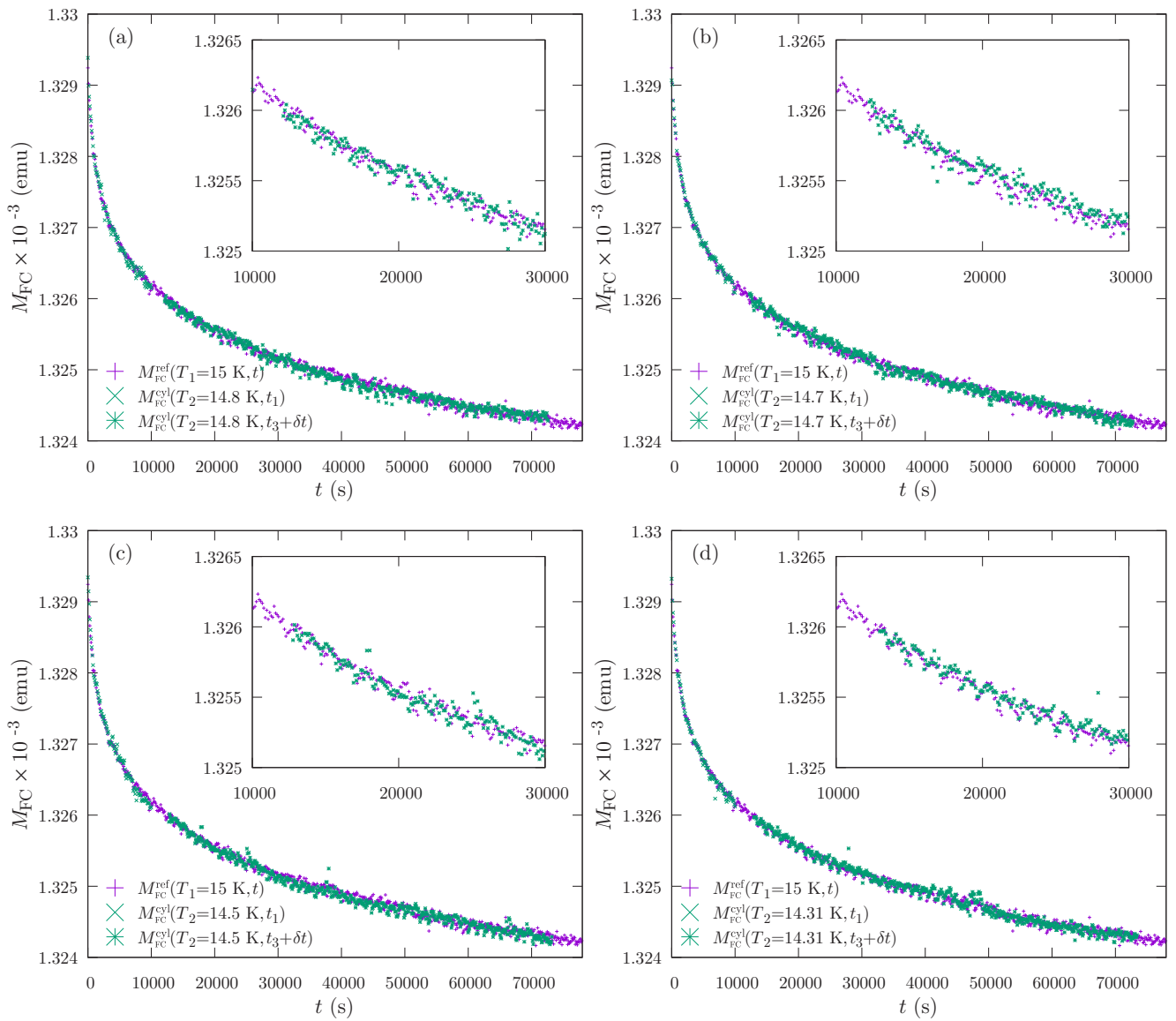


FIG. 9.  $T$ -cycling experiment results at  $T_1 = 15 \text{ K}$ . Cumulative aging is exhibited in plots (a)–(d); noncumulative aging is shown in plots (e)–(g). The reversible temperature range is approximately 690 mK.

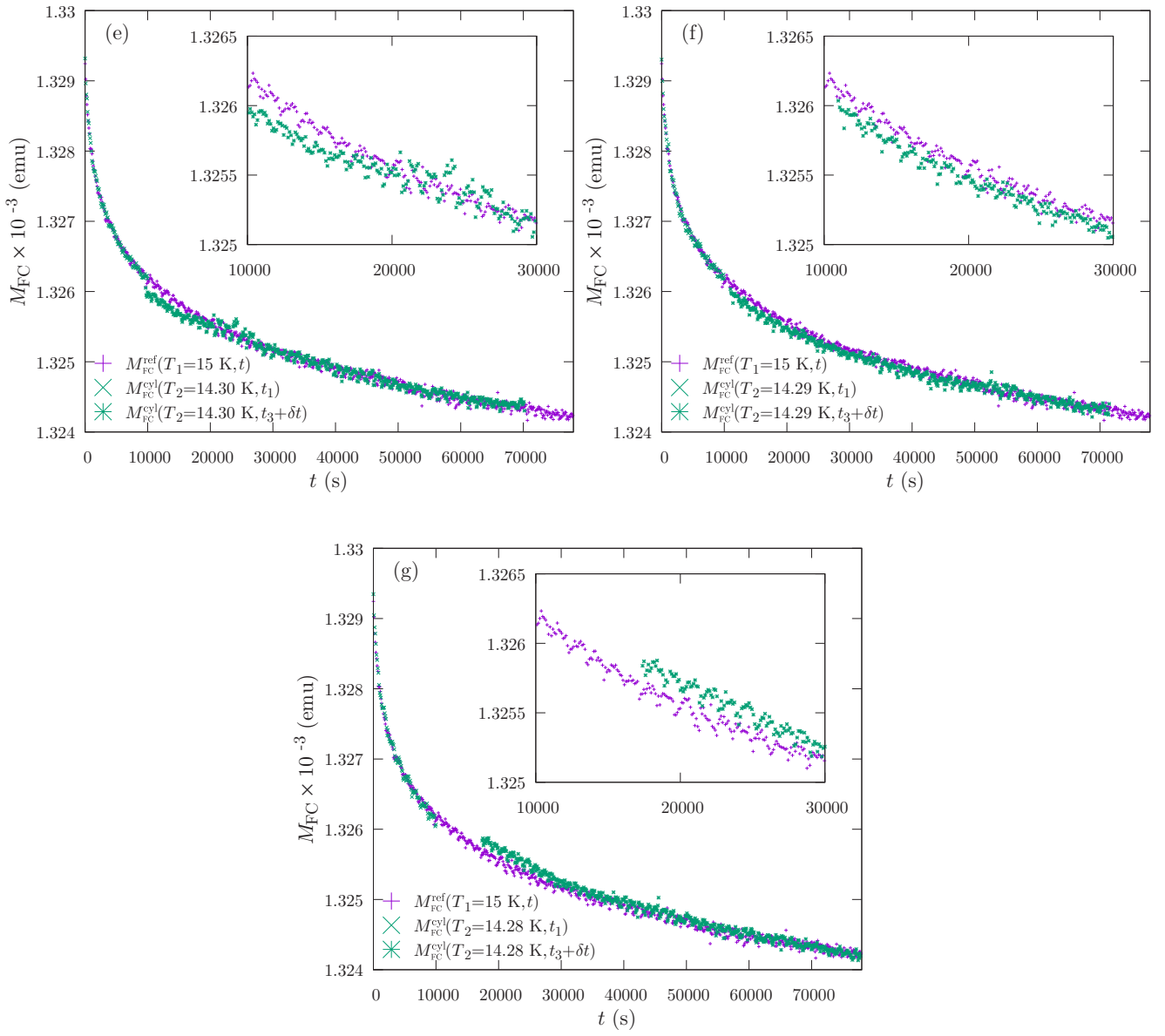


FIG. 9. (Continued.)

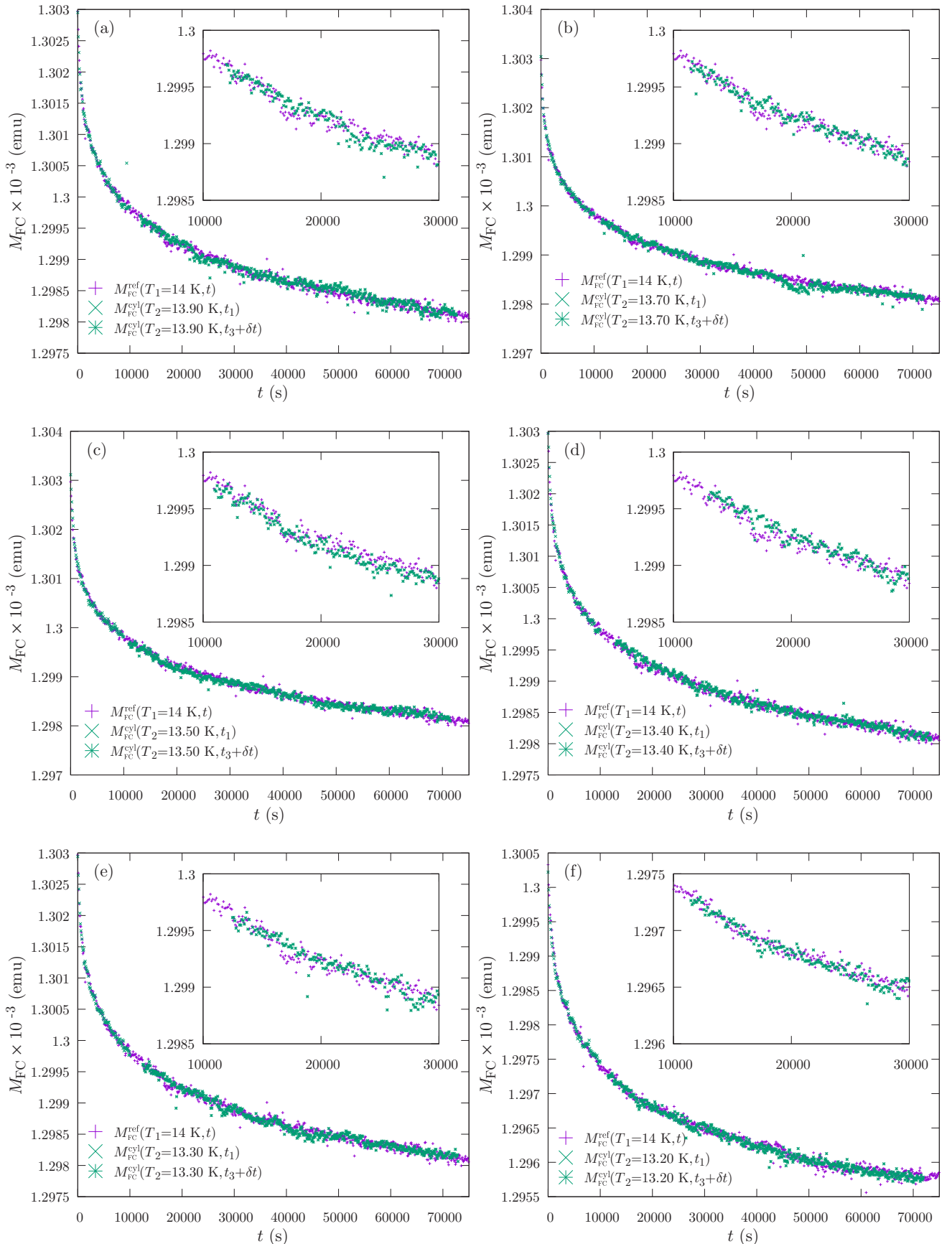


FIG. 10.  $T$ -cycling experiment results at  $T_1 = 14$  K. Cumulative aging is seen for plots (a)–(f); noncumulative aging is shown in plots (g)–(i). The reversible temperature range is approximately 800 mK.

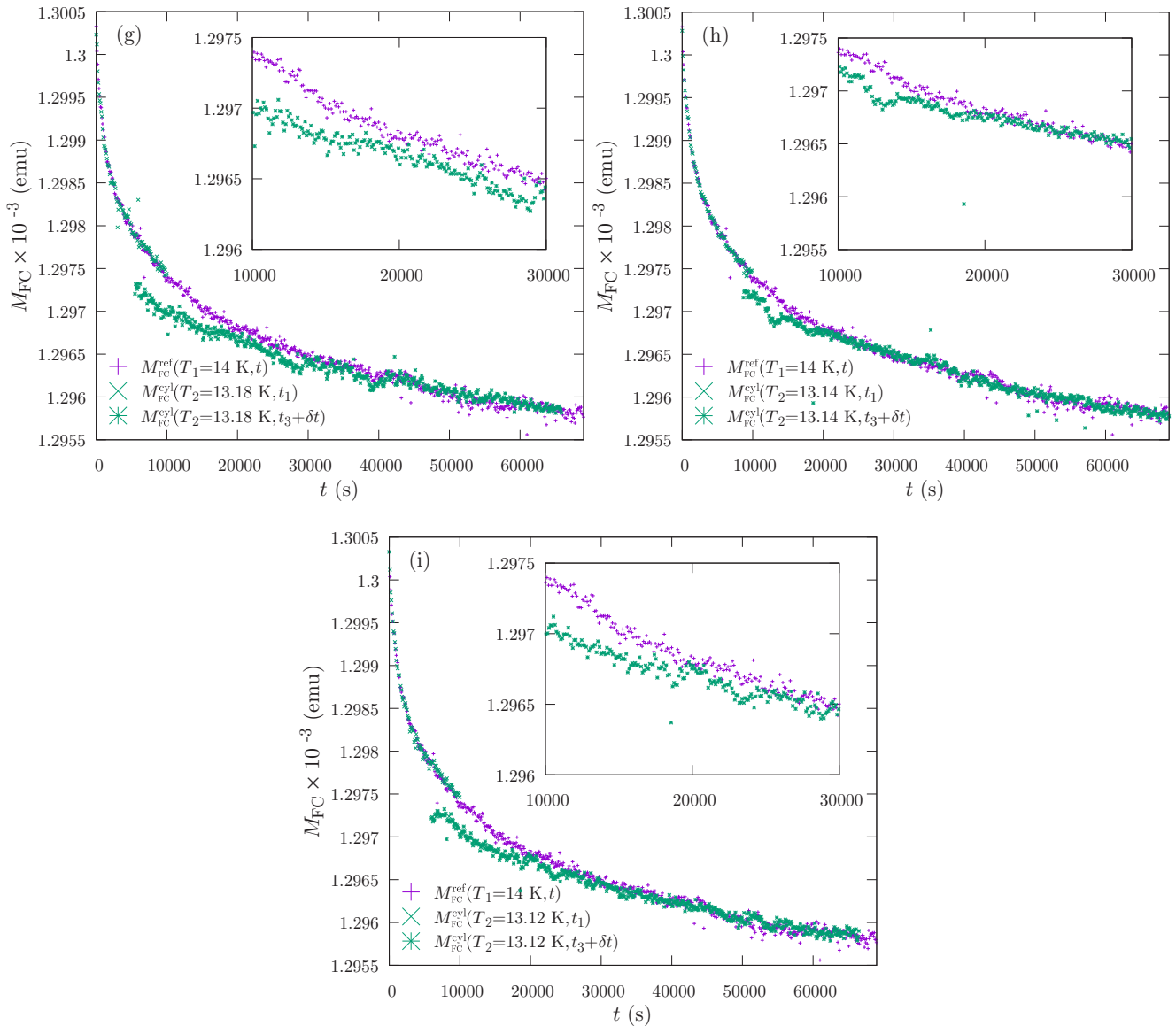


FIG. 10. (Continued.)

- [1] M. Mézard, G. Parisi, and M. A. Virasoro, *Spin Glass Theory and Beyond: An Introduction to the Replica Method and Its Applications*, Vol. 9 (World Scientific Publishing Company, 1987).
- [2] D. S. Fisher and D. A. Huse, *Phys. Rev. Lett.* **56**, 1601 (1986).
- [3] D. S. Fisher and D. A. Huse, *Phys. Rev. B* **38**, 386 (1988).
- [4] A. J. Bray and M. A. Moore, *Phys. Rev. Lett.* **58**, 57 (1987).
- [5] S. R. McKay, A. N. Berker, and S. Kirkpatrick, *Phys. Rev. Lett.* **48**, 767 (1982).
- [6] J. R. Banavar and A. J. Bray, *Phys. Rev. B* **35**, 8888 (1987).
- [7] M. Nifle and H. J. Hilhorst, *Phys. Rev. Lett.* **68**, 2992 (1992).
- [8] I. Kondor and A. Vegso, *J. Phys. A: Math. Gen.* **26**, L641 (1993).
- [9] M. Ney-Nifle and H. Hilhorst, *Physica A* **193**, 48 (1993).
- [10] L. F. Cugliandolo and J. Kurchan, *Phys. Rev. B* **60**, 922 (1999).
- [11] T. Rizzo and H. Yoshino, *Phys. Rev. B* **73**, 064416 (2006).
- [12] P. Barucca, G. Parisi, and T. Rizzo, *Phys. Rev. E* **89**, 032129 (2014).
- [13] D. Panchenko, *Commun. Math. Phys.* **346**, 703 (2016).
- [14] W.-K. Chen and D. Panchenko, *J. Stat. Phys.* **166**, 1151 (2017).
- [15] G. B. Arous, E. Subag, and O. Zeitouni, *Commun. Pure Appl. Math.* **73**, 1732 (2020).
- [16] R. Eldan, *J. Stat. Phys.* **181**, 1266 (2020).
- [17] H. Rieger, L. Santen, U. Blasum, M. Diehl, M. Jünger, and G. Rinaldi, *J. Phys. A: Math. Gen.* **29**, 3939 (1996).
- [18] M. Ney-Nifle and A. P. Young, *J. Phys. A: Math. Gen.* **30**, 5311 (1997).
- [19] M. Ney-Nifle, *Phys. Rev. B* **57**, 492 (1998).
- [20] S. T. Almeida, E. M. Curado, and F. D. Nobre, *J. Stat. Mech.: Theory Exp.* (2013) P06013.
- [21] M. Cieplak, M. S. Li, and J. R. Banavar, *Phys. Rev. B* **47**, 5022 (1993).
- [22] D. A. Huse and L.-F. Ko, *Phys. Rev. B* **56**, 14597 (1997).
- [23] M. Sasaki and K. Nemoto, *J. Phys. Soc. Jpn.* **69**, 2283 (2000).
- [24] H. Yoshino, A. Lemaitre, and J.-P. Bouchaud, *Eur. Phys. J. B* **20**, 367 (2001).
- [25] F. Krzakala, *Europhys. Lett. (EPL)* **66**, 847 (2004).

- [26] J. Lukic, E. Marinari, O. C. Martin, and S. Sabatini, *J. Stat. Mech.: Theory Exp.* (2006) L10001.
- [27] G. Parisi and T. Rizzo, *J. Phys. A: Math. Theor.* **43**, 235003 (2010).
- [28] C. K. Thomas, D. A. Huse, and A. A. Middleton, *Phys. Rev. Lett.* **107**, 047203 (2011).
- [29] Y. Sun, A. Crisanti, F. Krzakala, L. Leuzzi, and L. Zdeborová, *J. Stat. Mech.: Theory Exp.* (2012) P07002.
- [30] A. Billoire and E. Marinari, *Europhys. Lett.* **60**, 775 (2002).
- [31] F. Krzakala and O. Martin, *Eur. Phys. J. B* **28**, 199 (2002).
- [32] H. G. Katzgraber and F. Krzakala, *Phys. Rev. Lett.* **98**, 017201 (2007).
- [33] T. Jörg and F. Krzakala, *J. Stat. Mech.: Theory Exp.* (2012) L01001.
- [34] L. A. Fernandez, V. Martin-Mayor, G. Parisi, and B. Seoane, *Europhys. Lett.* **103**, 67003 (2013).
- [35] A. Billoire, *J. Stat. Mech.: Theory Exp.* (2014) P04016.
- [36] W. Wang, J. Machta, and H. G. Katzgraber, *Phys. Rev. B* **92**, 094410 (2015).
- [37] A. Billoire, L. A. Fernandez, A. Maiorano, E. Marinari, V. Martin-Mayor, J. Moreno-Gordo, G. Parisi, F. Ricci-Tersenghi, and J. J. Ruiz-Lorenzo, *J. Stat. Mech.: Theory Exp.* (2018) 033302.
- [38] H. Yoshino, *J. Phys. A: Math. Gen.* **36**, 10819 (2003).
- [39] M. Sasaki and O. C. Martin, *Phys. Rev. Lett.* **91**, 097201 (2003).
- [40] H. Takayama, *J. Magn. Magn. Mater.* **272-276**, 256 (2004), Proceedings of the International Conference on Magnetism (ICM 2003).
- [41] M. Sasaki, K. Hukushima, H. Yoshino, and H. Takayama, *Phys. Rev. Lett.* **95**, 267203 (2005).
- [42] M. Sasaki and O. C. Martin, *Europhys. Lett.* **60**, 316 (2002).
- [43] T. Rizzo and A. Crisanti, *Phys. Rev. Lett.* **90**, 137201 (2003).
- [44] M. Baity-Jesi, E. Calore, A. Cruz, L. A. Fernandez, J. M. Gil-Narvion, I. G.-A. Pearnin, A. Gordillo-Guerrero, D. Iñiguez, A. Maiorano, E. Marinari *et al.*, *Commun. Phys.* **4**, 74 (2021).
- [45] L. Sandlund, P. Svedlindh, P. Granberg, P. Nordblad, and L. Lundgren, *J. Appl. Phys.* **64**, 5616 (1988).
- [46] J. Mattsson, C. Djurberg, P. Nordblad, L. Hoines, R. Stubi, and J. A. Cowen, *Phys. Rev. B* **47**, 14626 (1993).
- [47] K. Jonason, E. Vincent, J. Hammann, J. P. Bouchaud, and P. Nordblad, *Phys. Rev. Lett.* **81**, 3243 (1998).
- [48] T. Jonsson, K. Jonason, P. Jönsson, and P. Nordblad, *Phys. Rev. B* **59**, 8770 (1999).
- [49] P. E. Jönsson, H. Yoshino, and P. Nordblad, *Phys. Rev. Lett.* **89**, 097201 (2002).
- [50] R. Arai, K. Komatsu, and T. Sato, *Phys. Rev. B* **75**, 144424 (2007).
- [51] G. B. Alers, M. B. Weissman, and N. E. Israeloff, *Phys. Rev. B* **46**, 507 (1992).
- [52] T. Komori, H. Yoshino, and H. Takayama, [arXiv:cond-mat/0001395](https://arxiv.org/abs/cond-mat/0001395) (2000).
- [53] J.-P. Bouchaud, V. Dupuis, J. Hammann, and E. Vincent, *Phys. Rev. B* **65**, 024439 (2001).
- [54] L. Berthier and J.-P. Bouchaud, *Phys. Rev. Lett.* **90**, 059701 (2003).
- [55] F. Lefloch, J. Hammann, M. Ocio, and E. Vincent, *Europhys. Lett.* **18**, 647 (1992).
- [56] E. Vincent, J. P. Bouchaud, J. Hammann, and F. Lefloch, *Philos. Mag. B* **71**, 489 (1995).
- [57] M. Picco, F. Ricci-Tersenghi, and F. Ritort, *Eur. Phys. J. B* **21**, 211 (2001).
- [58] M. Suzuki and I. Suzuki, *Eur. Phys. J. B* **41**, 457 (2004).
- [59] E. Vincent, V. Dupuis, M. Alba, J. Hammann, and J.-P. Bouchaud, *Europhys. Lett.* **50**, 674 (2000).
- [60] E. Vincent, J. Hammann, and M. Ocio, *J. Stat. Phys.* **135**, 1105 (2009).
- [61] K. Jonason, P. Nordblad, E. Vincent, J. Hammann, and J.-P. Bouchaud, *Eur. Phys. J. B* **13**, 99 (2000).
- [62] R. Mathieu, P. E. Jönsson, P. Nordblad, H. A. Katori, and A. Ito, *Phys. Rev. B* **65**, 012411 (2001).
- [63] M. Sasaki, V. Dupuis, J.-P. Bouchaud, and E. Vincent, *Eur. Phys. J. B* **29**, 469 (2002).
- [64] F. Scheffler, H. Yoshino, and P. Maass, *Phys. Rev. B* **68**, 060404(R) (2003).
- [65] P. E. Jönsson, H. Yoshino, and P. Nordblad, *Phys. Rev. Lett.* **90**, 059702 (2003).
- [66] P. E. Jönsson, R. Mathieu, P. Nordblad, H. Yoshino, H. A. Katori, and A. Ito, *Phys. Rev. B* **70**, 174402 (2004).
- [67] L. Berthier and P. C. W. Holdsworth, *Europhys. Lett.* **58**, 35 (2002).
- [68] L. Berthier and J.-P. Bouchaud, *Phys. Rev. B* **66**, 054404 (2002).
- [69] M. Sales, J.-P. Bouchaud, and F. Iix Ritort, *J. Phys. A: Math. Gen.* **36**, 665 (2003).
- [70] L. Berthier and A. P. Young, *Phys. Rev. B* **71**, 214429 (2005).
- [71] F. Krzakala and F. Ricci-Tersenghi, *J. Phys.: Conf. Ser.* **40**, 42 (2006).
- [72] T. Aspelmeier, A. J. Bray, and M. A. Moore, *Phys. Rev. Lett.* **89**, 197202 (2002).
- [73] M. Picco, F. Ricci-Tersenghi, and F. Ritort, *Phys. Rev. B* **63**, 174412 (2001).
- [74] H. Takayama and K. Hukushima, *J. Phys. Soc. Jpn.* **71**, 3003 (2002).
- [75] D. McNamara, A. A. Middleton, and C. Zeng, *Phys. Rev. B* **60**, 10062 (1999).
- [76] M. Sales and H. Yoshino, *Phys. Rev. E* **65**, 066131 (2002).
- [77] R. A. da Silveira and J.-P. Bouchaud, *Phys. Rev. Lett.* **93**, 015901 (2004).
- [78] P. Le Doussal, *Phys. Rev. Lett.* **96**, 235702 (2006).
- [79] S. Kustov, I. Liubimova, M. Corró, J. Torrens-Serra, X. Wang, C. R. Haines, and E. K. Salje, *Sci. Rep.* **9**, 5076 (2019).
- [80] R. Daviet and N. Dupuis, *Phys. Rev. E* **103**, 052136 (2021).
- [81] H. G. Katzgraber, F. Hamze, Z. Zhu, A. J. Ochoa, and H. Munoz-Bauza, *Phys. Rev. X* **5**, 031026 (2015).
- [82] V. Martin-Mayor and I. Hen, *Sci. Rep.* **5**, 15324 (2015).
- [83] W. Vinci, T. Albash, G. Paz-Silva, I. Hen, and D. A. Lidar, *Phys. Rev. A* **92**, 042310 (2015).
- [84] Z. Zhu, A. J. Ochoa, S. Schnabel, F. Hamze, and H. G. Katzgraber, *Phys. Rev. A* **93**, 012317 (2016).
- [85] J. Hammann, M. Lederman, M. Ocio, R. Orbach, and E. Vincent, *Physica A* **185**, 278 (1992).
- [86] H. Rieger, B. Steckemetz, and M. Schreckenberg, *Europhys. Lett.* **27**, 485 (1994).
- [87] C. Djurberg, K. Jonason, and P. Nordblad, *Eur. Phys. J. B* **10**, 15 (1999).
- [88] P. Granberg, L. Sandlund, P. Nordblad, P. Svedlindh, and L. Lundgren, *Phys. Rev. B* **38**, 7097 (1988).
- [89] P. Granberg, L. Lundgren, and P. Nordblad, *J. Magn. Magn. Mater.* **92**, 228 (1990).

- [90] R. Mathieu, M. Hudl, and P. Nordblad, *Europhys. Lett.* **90**, 67003 (2010).
- [91] I. Kondor, *J. Phys. A: Math. Gen.* **22**, L163 (1989).
- [92] A. Billoire and B. Coluzzi, *Phys. Rev. E* **67**, 036108 (2003).
- [93] M. Alba, M. Ocio, and J. Hammann, *Europhys. Lett.* **2**, 45 (1986).
- [94] F. Bert, V. Dupuis, E. Vincent, J. Hammann, and J.-P. Bouchaud, *Phys. Rev. Lett.* **92**, 167203 (2004).
- [95] Q. Zhai, D. C. Harrison, and R. L. Orbach, *Phys. Rev. B* **96**, 054408 (2017).
- [96] Q. Zhai, V. Martin-Mayor, D. L. Schlagel, G. G. Kenning, and R. L. Orbach, *Phys. Rev. B* **100**, 094202 (2019).
- [97] Q. Zhai, D. C. Harrison, D. Tennant, E. D. Dahlberg, G. G. Kenning, and R. L. Orbach, *Phys. Rev. B* **95**, 054304 (2017).
- [98] P. E. Jönsson, H. Yoshino, P. Nordblad, H. Aruga Katori, and A. Ito, *Phys. Rev. Lett.* **88**, 257204 (2002).
- [99] M. Baity-Jesi, E. Calore, A. Cruz, L. A. Fernandez, J. M. Gil-Narvion, A. Gordillo-Guerrero, D. Iñiguez, A. Maiorano, E. Marinari, V. Martin-Mayor, J. Moreno-Gordo, A. Muñoz Sudupe, D. Navarro, G. Parisi, S. Perez-Gaviro, F. Ricci-Tersenghi, J. J. Ruiz-Lorenzo, S. F. Schifano, B. Seoane, A. Tarancon, R. Tripiccion, and D. Yllanes (Janus Collaboration), *Phys. Rev. Lett.* **120**, 267203 (2018).
- [100] S. Feng, A. J. Bray, P. A. Lee, and M. A. Moore, *Phys. Rev. B* **36**, 5624 (1987).
- [101] V. Dupuis, E. Vincent, J.-P. Bouchaud, J. Hammann, A. Ito, and H. A. Katori, *Phys. Rev. B* **64**, 174204 (2001).
- [102] V. Martin-Mayor and S. Perez-Gaviro, *Phys. Rev. B* **84**, 024419 (2011).
- [103] M. Baity-Jesi, L. A. Fernández, V. Martín-Mayor, and J. M. Sanz, *Phys. Rev. B* **89**, 014202 (2014).
- [104] Q. Zhai, I. Paga, M. Baity-Jesi, E. Calore, A. Cruz, L. A. Fernandez, J. M. Gil-Narvion, I. Gonzalez-Adalid Pemartin, A. Gordillo-Guerrero, D. Iñiguez, A. Maiorano, E. Marinari, V. Martin-Mayor, J. Moreno-Gordo, A. Muñoz Sudupe, D. Navarro, R. L. Orbach, G. Parisi, S. Perez-Gaviro, F. Ricci-Tersenghi *et al.*, *Phys. Rev. Lett.* **125**, 237202 (2020).
- [105] I. Paga, Q. Zhai, M. Baity-Jesi, E. Calore, A. Cruz, L. A. Fernandez, J. M. Gil-Narvion, I. G.-A. Pemartin, A. Gordillo-Guerrero, D. Iñiguez, A. Maiorano, E. Marinari, V. Martin-Mayor, J. Moreno-Gordo, A. Muñoz-Sudupe, D. Navarro, R. L. Orbach, G. Parisi, S. Perez-Gaviro, F. Ricci-Tersenghi *et al.*, *J. Stat. Mech.: Theory Exp.* (2021) 033301.
- [106] W. Wang, M. Wallin, and J. Lidmar, *Phys. Rev. E* **98**, 062122 (2018).

*Correction:* The omission of a support statement in the Acknowledgment section has been fixed.